JCAMECH

Vol. 50, No. 2, December 2019, pp 366-374
DOI: 10.22059/jcamech.2019.270110.345

The Effect of Short-Range Type C and B UV Radiation on the Mechanical Properties of Skin Fibroblasts

Amirhossein Azami[a], *Ashkan Heydarian*[a,*], *Armin Jarahi Khameneh*[a], *Siamak Khoramymehr*[a], *Behnoush Vasaghi Gharamaleki*[b]

[a] *Department of Biomedical Engineering, Science and Research Branch, Islamic Azad University, Tehran, Iran*
[b] *Department of Basic Sciences of Rehabilitation, Iran University of Medical Sciences (IUMS), Tehran, Iran*

ARTICLE INFO

Article history:
Received: 22 October 2018
Accepted: 29 September 2019

Keywords:
Ultraviolet Effects
Cell Biomechanics
Creep Response
Viscoelastic

ABSTRACT

The effect of UV beam, which has been emitted from a natural or a manmade source on cells has been studied in previous studies for several times. Radiation of this beam can have different effects on DNA of the cell, cytotoxicity, the structure of cellular proteins and their mechanical properties based on radiation period or frequency. The effect of radiation of two types of beams, namely UVB and UVC on stiffness and deformation of the cell are studied in such studies based on different durations of radiation. Viscoelastic properties of skin fibroblast cells were measured using the magnetic tweezer method for a number of groups under UVC radiation with radiation durations of 38, 60 and 120 seconds and for a group under UVB radiation with radiation duration of 38 seconds, also for a control group. In addition, three and four-element discrete differential models were used for creep analysis. Cells deformation had a considerable change after radiation, while such deformation decreased as the frequency increased, however, no comment can be stated regarding radiation duration. Furthermore, cell stiffness reduced after radiation. Such decrease in cell stiffness after radiation could be due to the destruction of the biological macromolecule's bonds. Furthermore, the extent of cell deformation was much lower in the radiation groups in comparison to the control group.

1. Introduction

Skin is the largest organ of the body, covering a surface area about 1.6 to 2 m^2 of the body; on average, it comprises about 15% of the body weight. Skin is the outermost body layer and is in charge of duties such as protecting the internal tissues, preventing the introduction of pathogenic factors, and regulating body temperature. Generally, the skin is comprised of three main layers called epidermis, dermis, and hypodermis [1-4].

One of the important factors that directly influences the health of skin tissues is UV radiation by the Sun [5-7]. Recent studies have indicated that UV radiation can lead to skin diseases and problems including erythema, edema, sunburn, hyperplasia, immune suppression, DNA damage, and melanoma [8-12].

UV radiation, as a part of solar radiation, includes an extensive range of different wavelengths. Sun UV radiation is divided into three categories called UVA, UVB, and UVC. UVA, which has a wavelength between 320 and 400 nm, accounts for 90%- 95% of the radiation reaching the surface of the earth and can cause color changes or even death of skin cells. UVB, with a wavelength between 290 and 320 nm, accounts for 4% to 5% of the UV radiation reaching the surface of the earth and can lead to many biological changes in the skin including the formation of free radicals and melanoma. In the end, UVC, with a wavelength between 210 to 290 nm, claims the minimum UV radiation of the sun which is generally absorbed by the atmosphere of the earth. However, even short-term radiation of UVC can cause serious problems such as severe burnings or effects on DNA and even melanoma. UVC radiation can occur even by artificial sources such as sterilizing lamps and mercury lamps as well [8, 10, 13-15].

Nowadays, several studies have been conducted on the effects of various types of UV radiation on the skin. According to many papers, UVB and UVC radiation can have a significant effect on the mechanical properties of the skin [16-19].

For instance, Yasutomo Nishimori et *al*. [20] studied the effect of UV radiation on the mechanical properties of the skin of humans and mice in a research through examining the effects of radiation on skin collagen fiber bundles. The radiation utilized in their experiment was comprised of 60% UVC at a wavelength of 260-280 nm, 72.7% UVB at a wavelength of 280-320 nm, and 26.7% UVA at a wavelength of 320-400 nm. The mechanical properties of human and mouse skins, studied in that experiment, were measured utilizing a Cutometer SEM 474, a suction extensometer. The results indicated that the mechanical properties diminished in the radiated group in comparison to the normal group; such a reduction led to decreased elasticity of the skin in the radiated group in comparison to the normal group.

In another study, Bertrand Vileno et *al*. [13] studied the effects of UVA and UVC radiations on the elasticity of fibroblast cells. In

* Ashkan Heydarian. Tel.: +98 917 315 9532; e-mail: a.heydarian@srbiau.ac.ir

that study, UVC radiation was conducted at a wavelength of 254 nm and UVA radiation was conducted at a wavelength of 365 nm. Furthermore, elasticity was measured using Atomic Force Microscopy (AFM) method. The results of this study indicated that UVC radiation for 120 seconds led to 75% reduction of Young's modulus of these cells.

Y. Takema & G. [21] Imokava also conducted another research, where they used two radiations called a UVA ray at a wavelength of 351 nm and a UVB ray at a wavelength of 312 nm. They used a Cutometer SEM 474 for measuring the elasticity of the skin. The results of their study showed a significant decrease in the elasticity after UVB radiation.

Further, Devasier Benneta and Sanghyo Kim [16] aimed to study the normal, pathological, and protective role of UV radiation on three different types of skin cells (human keratinocyte, melanocyte, and fibroblast cell lines). They also dealt with finding the morphological, biophysical, and biomechanical changes under certain UV radiations. They implemented a UV radiation with a wavelength of 254-365 nm. Further, they conducted their analysis of the cell's roughness and stiffness based on the results through a Bio-AFM. The outcome of their research proved the significant alternation of biomechanical properties of the cells under UV exposure. The irradiated cells indicated increased roughness and stiffness.

In addition, Krysta Biniek et *al*. [22] conducted research to uncover the probable negative effect of both UVB and UVA on human skin cells. They focused their investigation on the Stratum Corneum (SC) which is the outermost layer of the skin. Both narrowband and broadband UVB radiation sources were chosen for the radiation procedure of their experiment. Further, for the biomechanical test, they planned to conduct micro tension bulge and double cantilever beam. The final result of their study proved the adverse effect of UVB radiation on the mechanical integrity of skin cells on of the SCs which could negatively affect the mechanical resilience of the skin.

The importance of such changes in mechanical properties is that our body cells undergo physiological changes under the effect of physical and chemical changes. Therefore, an effective method for diagnosing healthy cells from diseased cells is to determine the biochemical and biomechanical properties of them. Until now, the effects of such chemical and mechanical factors have been identified in many intracellular processes, such as gene expression, cell division, cell migration, and metabolic activity [23-25]. Recent research has indicated the effect of such chemical and mechanical factors on alterations of pathologic properties [26, 27].

One of the most important mechanical properties is the viscoelastic properties of cells; any changes to these properties can indicate structural and molecular changes due to the start or progression of disease in the body [28-30].

In this study, we have investigated the effect of short-term UVC radiation at a wavelength of 254 nm and UVB radiation at a wavelength of 312 nm on the viscoelastic properties of skin fibroblast cells utilizing the magnetic tweezer method. Initially, the samples were cultivated by the Iranian Biological Research Center (IRBC). Then, at the final stages of cultivation, Nano Magnetic Beads functionalized by folic acid were added to the cell cultivation plates. In the next stage, the cells were divided into five separate groups with different radiation durations and frequencies including UVB radiation for 38 seconds, UVC radiation for 38 seconds, UVC radiation for 60 seconds, and UVC radiation for 120 seconds. The cells were then loaded utilizing a magnetic tweezer device. Next, the data were extracted via image processing of the recorded videos and then processed accordingly. Thereafter, in order to determine the effects of UV radiations, appropriate mechanical models were attributed to them in order to study the creep behavior of cells with different exposure durations and frequencies. Our initial hypothesis in this experiment was that UV radiation for longer durations and higher frequencies causes decreased cell stiffness. Indeed, our expectation at the beginning of the experiment was obtaining results which could prove reduced deformation and stiffness of the cells in the groups under radiation. It was also expected that the groups under longer radiation durations and higher frequencies should experience far dramatic changes in deformation and stiffness. Such expectation came from the fact that longer UV radiation times and higher radiation frequencies will increase the ultimate UV dose (UV dose = UV intensity (W/cm^2) × Exposure duration (s)) which can negatively damage the cell structure. Several previous studies have established such a relationship. For instance, Vileno et *al*. [13] discovered that longer UVC radiation can cause greater reduction of Young's Modulus compared to the UVA radiation with the exact same radiation time. Further, they observed the destructive impact of longer radiation duration in reducing the Young's Modulus of the cells.

2. Materials and Methods

2.1. Cell Line

All of the experiments were conducted on (Hu02) Human Fibroblast cell line. The cells were cultivated by IBRC under specific conditions (at the temperature of 37°C, CO_2 by 5 %, Air by 95%, and DMEM and FBS by 10%). Then, by 0.25% Trypsin + 0.02 %, EDTA (3min; 37 ºC) was used for cell passaging of the samples where 10 Petri dishes were passaged with dimensions of 35×10 mm^2 of the cells. The mentioned Petri dishes were removed from the cultivation process once the number of cells reached 3×10^3 after which nano magnetic beads functionalized by folic acid from NanoZino Co., (Average Size: 10nM±5nM, 1000PPM, functionalized by folic acid) were added to the samples 4 hours prior to the experiment. Then, the samples were frozen in order to be transferred for the experiment (FBS +10% DMSO). Once the samples were transferred to the laboratory, they were divided into five separate groups including UVB38, UVC38, UVC60, UVC 120, and a control group. At the final stage and prior to the experiment, each of the Petri dishes was placed in an incubator for defrosting at the temperature of 37 °C and was then transferred under the laboratory hoods for completing further stages.

2.2. UV Radiation Source

Two separate lamps were used for this experiment: a radiation source of UVC (TUV T8) Lamp, Philips Co., Short-wave UV radiation with a peak at 253.7 nm (UVC), 20 W and a radiation source of UV-B Narrowband TL Lamp, Philips Co. Narrow waveband with a peak at 315 nm (UVB), 20 W. The lamps were fixed at the place of the experiment in a way that their horizontal and vertical distances from the samples were 10 cm and 50 cm, respectively.

2.3. Irradiation Protocol

Ten Petri dishes containing the samples were divided into five separate groups. The control group included two Petri dishes; UVB 38 included two Petri dishes under UVB radiation for 38 seconds; UVC38 included two Petri dishes under UVC radiation for 38 seconds; UVC60 included two Petri dishes under UVC radiation for 60 seconds; and UVC120 included two Petri dishes under UVC radiation for 120 seconds. Note that such radiation timings have been based on previous studies [13] so we can compare the results with previous findings. Furthermore, the UVB group was included in order to compare the radiation effects of UVB and UVC on the cells and their mechanical properties as well as their conformity with the previous studies. The control group was not exposed to UV radiation.

2.4. The Magnetic Tweezers Setup

The operation method of the magnetic tweezer device has been frequently described in previous papers and books [31, 32]. The device employed for this experiment was designed and manufactured by the experimental group consisting of separate components: a magnetic tip composed of a coil holder and a coil

with 1500 rounds of wire and width of 0.7 mm plus an Iron core. The imaging system that was used included a microscope (KM 1000, China) and a Webcam (5 megapixels, 60 frames per seconds) for capturing images and recording videos of the samples. Further, a laptop (ASUS K45VD-A) was used for saving and storing the images and videos as well as coordinating the recording timing and applying the mechanical load. Finally, the mechanic pulse maker device consisted of a generator (AFG3000, GW Instek, Taiwan) (Figure 1).

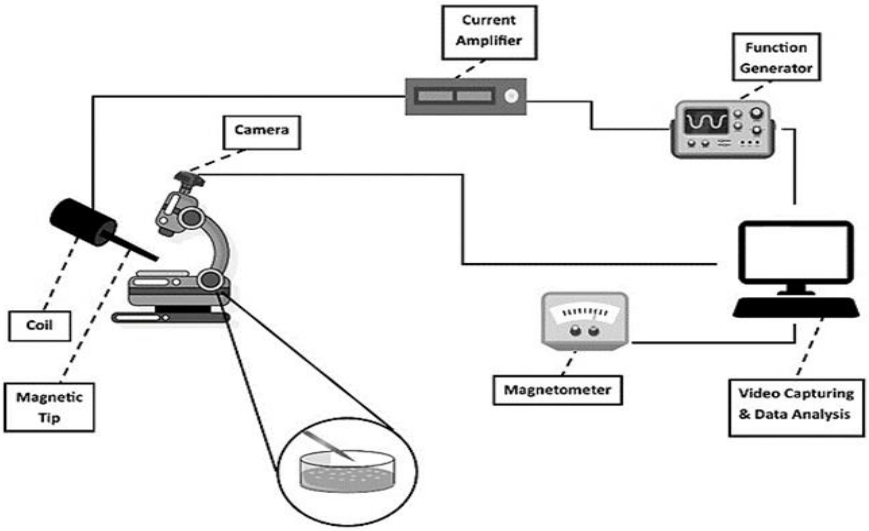

Figure 1. Schematic illustration of the magnetic tweezer setup; the setup includes different parts such as a microscope, camera, coil, magnetic tip, magnetometer, current amplifier, function generator, and a computer.

2.5. Calibration Method

The above-mentioned methods in the references and the previous studies were utilized for calibration of the device [32, 33].

2.6. Creep Response Evaluation and Data Analysis

Upon completion of the radiation protocol for each of the samples, the cell culture media of the Petri dishes were first removed using a micropipette and then the samples were placed under the magnetic tip for pre-conditioning. Pre-conditioning was comprised of 2.5 seconds loading and 2.5 seconds unloading after which the samples became ready for the experiment after 10 cycles. Then, the static creep test with a constant force of 299 pN was applied to the cells by the magnetic tip. In the next step, the images and videos of each of the experiments were captured and recorded by the imaging system for image processing and tracking. Subsequently, 5 cells were selected from each petri dish as the main sample for image processing and tracking. The TRACKER4.92 software (Open source tracking tool) was used for this purpose. At this stage, using specific filters, firstly the cell membrane was distinguished from the petri dish ambient, to prevent the formation of noise in the tracking process. The markers were placed on the cell membrane; the extent of deformation was calculated over loading times. The information about the samples included the extent of their deformation with their duration being categorized individually. Further, the values for mean and variance as well as the diagrams for deformation against time were obtained for each of the groups. The slope of the average deformation diagrams was considered at the creep section and then as an indicator of fluidity or solidity of the samples. A few models were selected first to find the best mechanical model with the minimum error. Then, based on the sample behaving like a fluid or solid, the best model with the minimum Root-Mean-Square-Error (RMSE) was considered as the main model through the curve fitting process. Next, the values for modulus of elasticity and damper were obtained for each of the models. Once the appropriate model was selected, the creep dynamic response of that model was used in order to obtain loss modulus and storage modulus.

3. Results

After drawing all diagrams of the average deformation against time (Fig. 2), which presented the deformation of the cells, the creep section of the diagram was determined through investigating the slopes of the diagram. If the slope is positive at the creep section, then the sample shows a fluid behavior, while if the slope is negative or zero, then it is an indicator of solidity. Accordingly, the control group, UVC38, UVC60, and UVC120 revealed a fluid behavior, while UVB38 displayed a solid behavior.

Once the behavior of the samples was clarified, it was the time for investigating the right mechanical models for the fluid and solid models as well as testing the static and dynamic states.

3.1. Static Experiment

Initially and for studying the behavior of the samples in a static state, curve fitting of the average deformation-time diagrams is essential to determine the most appropriate mechanical model for the fluid and solid groups. Mathematic 9 software was used for this purpose.

Further, we utilized the Root-Mean-Square-Error (RMSE) for determining the mechanical model with the minimum error. For that, the model presenting the minimum value for RMSE at curve fitting will be the most appropriate model. According to the calculations for the groups with the behavior of a fluid and a solid, the Burgers model and the Standard Linear Solid model respectively had the minimum value of RMSE; accordingly, these two models were selected as the best mechanical models for the samples.

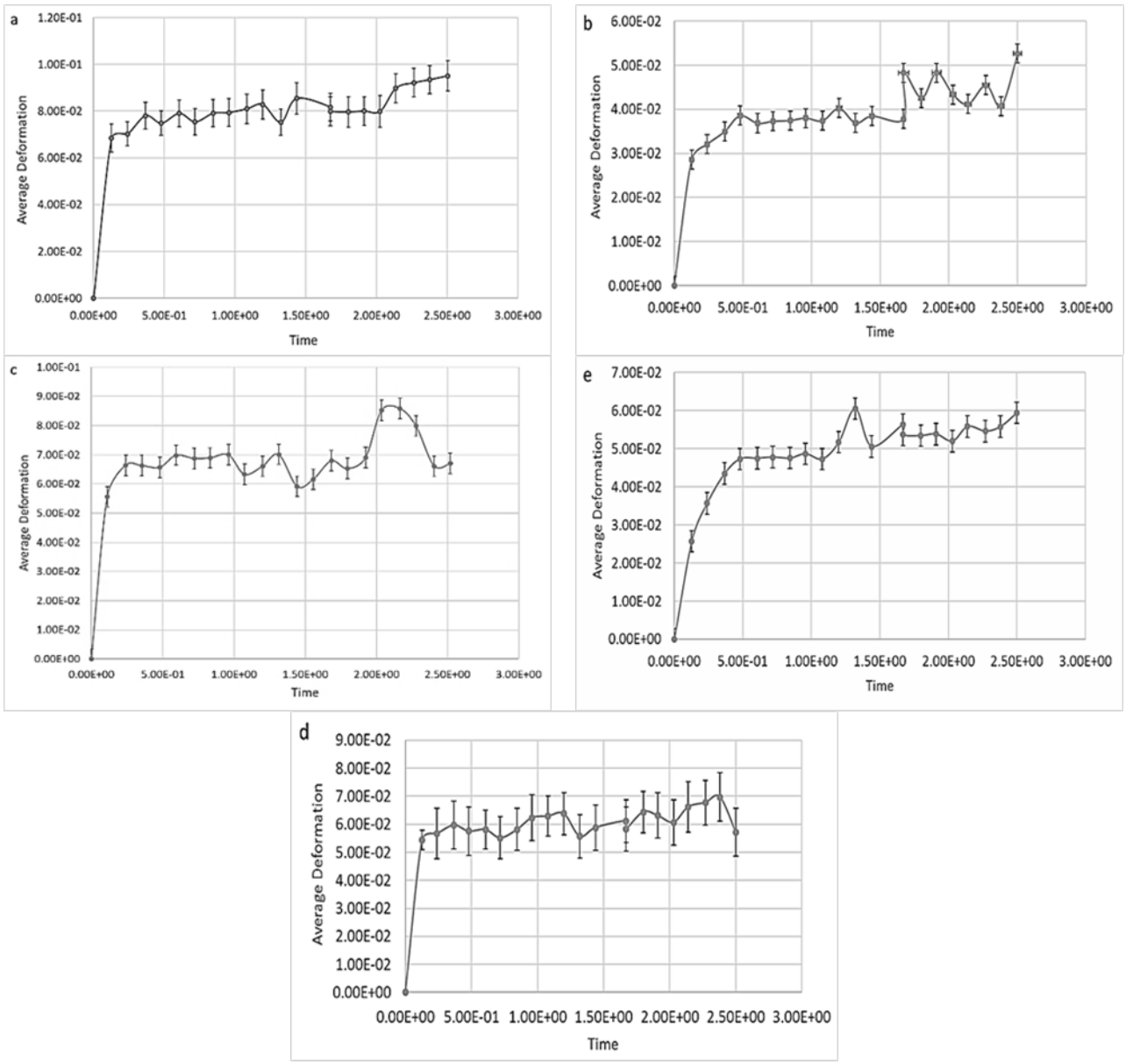

Figure 2. Diagrams of the average deformation against time from experimental results; a) Diagram of the control group with fluid behavior; b) Diagram of UVC38 group with fluid behavior; c) Diagram of UVC60 group with fluid behavior; d) Diagram of UVC120 group with fluid behavior; e) Diagram of UVB38 group with solid behavior.

The stress-strain equation for the Burgers model (Figure 3) with the behavior of fluid was obtained from the Eq. 1 [34] where E2 and E1 are the coefficients of springs, and η_1, η_2 represent the coefficients of dampers. In addition, the creep response of the Burgers model's differential equation was obtained from EQ.2.[34].

$$\sigma + (\frac{\eta_1}{E_1} + \frac{\eta_1}{E_2} + \frac{\eta_2}{E_2})\dot{\sigma} + \frac{\eta_1\eta_2}{E_1E_2}\ddot{\sigma} = \eta_1\dot{\varepsilon} + \frac{\eta_1\eta_2}{E_2}\ddot{\varepsilon} \quad (1)$$

$$\varepsilon(t) = \frac{\sigma_0}{E_1} + \frac{\sigma_0}{\eta_1}t + \frac{\sigma_0}{E_2}(1 - e^{-\frac{E_2}{\eta_2}t}) \quad (2)$$

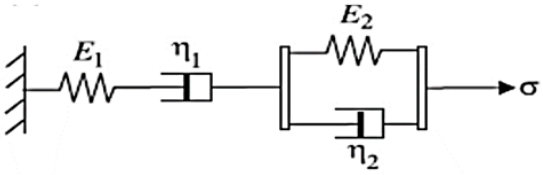

Figure 1. Schematic illustration of the Burgers model; E_1 and E_2 display the springs and η_1 ,η_2 denote the dampers [32-35].

Also, the stress-strain equation for the Standard Linear Solid model (Figure 4) with the behavior of a solid was obtained from Eq. 3 [34]; Where E_1 and E_2 represent the coefficients of springs and is the coefficient of the damper. In addition, the creep response of the differential equation of the Standard Linear Solid model was obtained from Eq. 4 [34]. In order to simplify the equation, we have used four parameters called p_1, q_1, q_0, and λ.

$$\sigma + \frac{\eta/E_1}{1+E_2/E_1}\dot{\sigma} = \frac{E_2}{1+E_2/E_1}\varepsilon + \frac{\eta}{1+E_2/E_1}\dot{\varepsilon} \quad (3)$$

$$\varepsilon(t) = \frac{\sigma_0}{\eta}\left[\frac{1}{\lambda}(1-e^{-\lambda t}) + p_1 e^{-\lambda t}\right]; \quad (4)$$

$$p_1 = \frac{\eta/E_1}{1+E_2/E_1}, q_0 = \frac{E_2}{1+E_2/E_1}, q_1 = \frac{\eta}{1+E_2/E_1}, \lambda = \frac{q_0}{q_1}$$

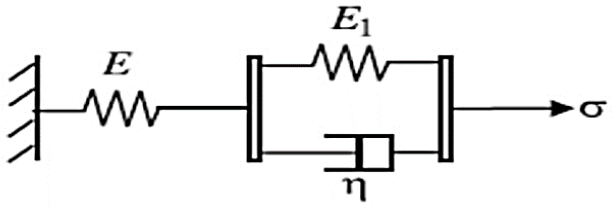

Figure 2. Schematic Illustration of the Standard Linear Solid model; E and E_1 display the springs and η shows the damper [33-36].

Curve fitting of the data in the diagram of average deformation against time for the stress-strain equation of the Burgers model with the behavior of fluid was conducted for the control group, UVC38, UVC60, and UVC 120 (Figures 5 a, b, c, d, respectively) via Mathematica 9 software. In addition, curve fitting of the data in the diagram of the average deformation against time for the stress-strain equation of the model with the behavior of a solid was conducted for UVB38 (Figure 5 e) again through Mathematica 9 software.

After the above steps, the values of spring and damper coefficients were calculated for the control group, UVC38, UVC60, UVC120, and UVB38, with the numerical values of such coefficients being presented in Table 1. Furthermore, the validity of the calculated values was confirmed by conducting a P test.

3.2. Dynamic Experiment

For studying the dynamic behavior of the samples, the diagrams associated with D* equation or the complex creep function should be drawn for each of the groups. For this purpose, D*equation is according to Eq. 5 for the groups with the behavior of fluid and according to Eq. 6 for the groups with the behavior of a solid. D* equation for both solids and fluids is comprised of a real part and an imaginary part which are drawn in two separate diagrams for each of the experimental groups (Figure 6) [37].

4. Discussion

The results obtained from drawing the diagrams of the average deformation against time for the five experiment groups which are displayed in Figure 2 indicate the behavior of the samples. The slope of the diagram of the average deformation against time at the section which reveals the creep behavior is indeed considered as an indicator for determination of the solidity or fluidity behavior of the sample.

The diagrams (Figure 2) depict the deformation property of the samples. It is possible to calculate the extent of deformation among the samples by calculating the maximum length changes. Accordingly, the value for deformation in Diagram a for the control group (during 2.5s) equals to 0.095 micrometer; in Diagram b for the group UVC120 (during 2.5 s) it equals to 0.07 micrometer; in Diagram c for the group UVC60 (during 2.5 s) equals to 0.085 micrometer; and in Diagram d for the group UVC38 (during 2.5 s) equals to 0.052 micrometer. In addition, Diagram e is the curve fitted diagram for the group UVB38 indicating deformation. The corresponding value of deformation in this diagram (during 2.5 s) equals 0.06 micrometer.

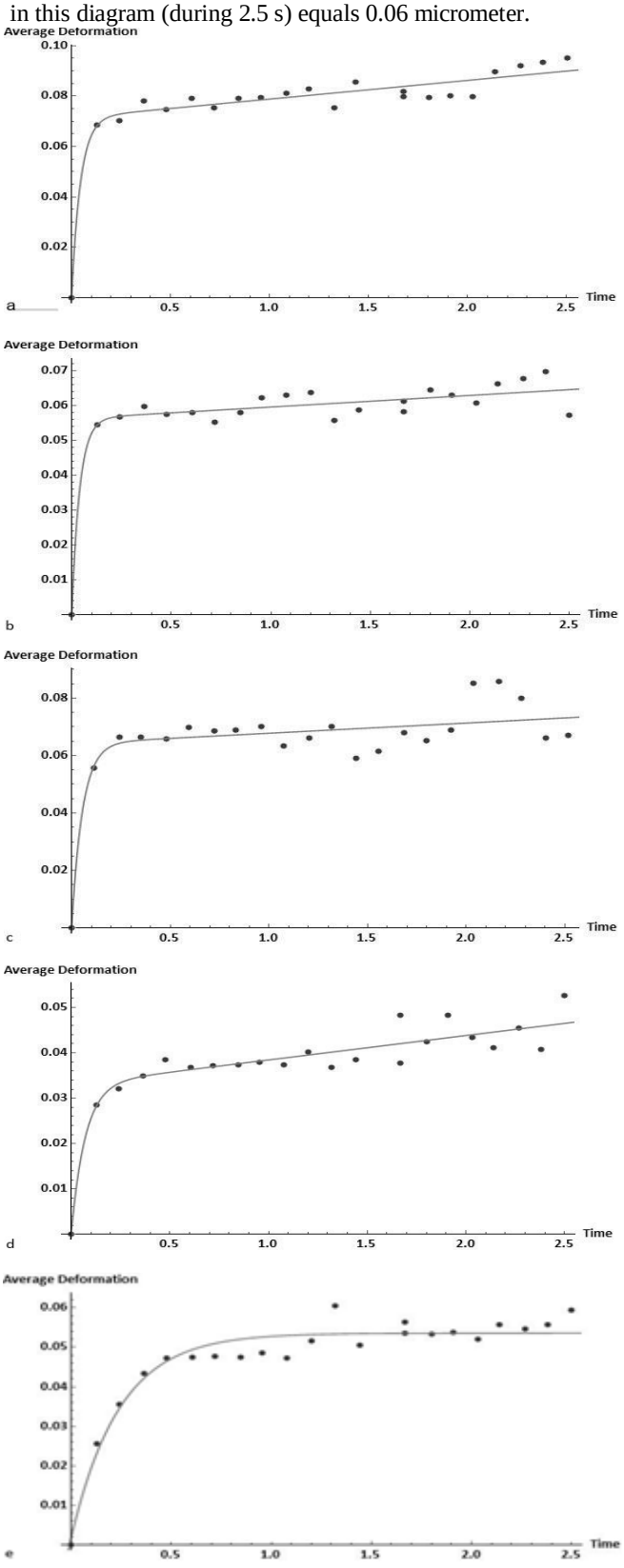

Figure 3. Curve fitted diagrams of average deformation against the time of samples; a) Diagram of the control group; b) Diagram of UVC120; c) Diagram of UVC60 group; d) Diagram of UVC38 group; e) Diagram of UVB38 group.

Table 1. Numerical values of spring and damper coefficients.

Coefficients	**Control**		**UVB38**		**UVC120**		**UVC60**		**UVC38**	
η_1 $\mu N \cdot s \cdot m^{-1}$	4.03466×10^4	P<0.05	–	–	8.97286	P<0.05	8.43342×10^4	P<0.05	5.56012×10^4	P<0.05
η_2 $\mu N \cdot s \cdot m^{-1}$	1.89735×10^2	P<0.05	1.38843×10^3	P<0.05	2.11491×10^2	P<0.05	2.58265×10^2	P<0.05	6.4513×10^2	P<0.05
E_1 $\mu N \cdot m^{-1}$	3.21657×10^7	P<0.05	1.68358×10^5	P<0.05	1.70089×10^9	P<0.05	2.89236×10^{12}	P<0.05	1.22713×10^7	P<0.05
E_2 $\mu N \cdot m^{-1}$	4.19205×10^3	P<0.05	5.77572×10^3	P<0.05	5.31828×10^3	P<0.05	4.65788×10^3	P<0.05	9.05365×10^3	P<0.05

$$D^*(\omega)=\left(\frac{1}{E_2}+\frac{E_2}{{E_2}^2\times{\eta^2}_2\times\omega}\right)-i\left(\frac{1}{\eta_1\times\omega}+\frac{\eta_2\times\omega}{{E_2}^2+{\eta_2}^2\times\omega^2}\right) \quad (5)$$

$$D^*(\omega)=\left(\frac{q_0+q_1p_1\times\omega^2}{{q_0}^2+{q_1}^2\times\omega^2}\right)-i\left(\frac{\omega(q_0p_1-q_1)}{{q_0}^2+{q_1}^2\times\omega^2}\right) \quad (6)$$

$$p_1=\frac{\eta/E_1}{1+E_2/E1},q_0=\frac{E_2}{1+E_2/E_1},q_1=\frac{\eta}{1+E_2/E_1}$$

According to the results, deformation of the cells begins to decline upon radiation. Deformation is indeed the ability of an object to be extended from its normal state. In the current study, all of the radiated groups displayed a significant reduction in comparison to the control group, which has been in line with our first hypothesis. The values of the maximum deformity of control, UVC38, UVC60, UVC120, and UVB38 are 0.095 ± 0.001 µM, 0.052 ± 0.001 µM, 0.085 ± 0.001 µM, 0.07 ± 0.001 µM, and 0.06 ± 0.001 µM respectively. These values reveal -0.45, -0.10, -0.26, and -0.36 reduction in the maximum deformity for UVC38, UVC60, UVC120, and UVB38, respectively, compared to the control group.

Furthermore, comparing the two UV radiation groups at different frequencies and same radiation duration, which are UVC and UVB radiated on the samples for 38 seconds, the cells exposed to the higher energetic radiation (i.e. UVC) had greater reduction in deformation (0.052 ± 0.001 µM) compared to the other group (0.06 ± 0.001 µM). This result is consistent with our hypothesis suggesting the effect of increased frequency on the reduction of deformation in the samples.

However, studying the effect of increased radiation duration for the UVC radiated groups, a similar effect is not observed for deformation. According to the primary hypothesis, the reduction of deformation was expected as the duration of radiation increases among the groups from 38 s to 120 s. Our results, however, indicated that increasing the duration of UVC radiation did not necessarily lead to reduced deformation.

Spring and damper coefficients for all of the groups including the normal group as well as UVC120, UVC60, UVC38, and UVB38 are presented in Table 1. Note that as the group UVB38 exhibits the behavior of a solid in contrast to the other four groups, therefore, it is not possible to compare its values for spring and damper coefficients with the same values of the other groups.

After drawing the diagrams for the dynamic state as provided in Figure 6, the frequency of 80 Hz was selected from each of the samples in order to investigate the stiffness of the samples. The selected frequency has been according to the normal frequency imposed on the skin as found by previous studies [38]. The stiffness of the samples is obtained from Eq. 7, wherein D* represents mixed dynamic modulus, D' denotes storage modulus, and D" shows loss modulus. The numerical values of stiffness for the different groups can be calculated by Eq. 8 [37]. Accordingly, the numerical values of stiffness at the frequency of 80 Hz for the groups are provided in Table 2.

$$D^*(\omega)=D'-iD \quad (7)$$

$$\left|D^*(\omega)\right|=\sqrt{(D')^2-(D'')^2} \quad (8)$$

In addition, based on Figure 6, it is possible to determine the behavior range of the fluid and solid for each of the samples. Accordingly, the Diagram a for the control group shows the behavior of a solid up to the frequency of 21.875 Hz after which it presents the behavior of a fluid. In Diagram b for the group UVC38, it reveals the behavior of a solid prior to the frequency of 13.589 Hz while after that, it exhibits the behavior of a fluid. In Diagram c for the UVC60, it indicates the behavior of solid prior to the frequency of 17.879 Hz and after that, it shows the behavior of the fluid. In Diagram d for the group UVC120, it demonstrates the behavior of a solid before the frequency of 24.526 after which it displays the behavior of a fluid. Finally, in Diagram e for the group UVB38, it depicts the behavior of a solid throughout the diagram. The procedure through which the cell apoptosis occurs after irradiation has been investigated with a bimolecular focus [39-43]. For instance, Chih-Hung Lee et *al*. [39] reported the actual effect of UV radiation on the course of cell apoptosis of the skin cells. They found that the UV radiation is responsible for the cell death in two separate ways including direct DNA damage and clustering of the cell death receptors on the surface of the cells. If the UV radiation causes the DNA damage (which normally happens under UVB/C radiation), the mitochondria will release cytochrome c to the cytosol which could eventually trigger the caspase release. This procedure could effectively trigger the cell apoptosis of the cells. Further, the UV radiation can cause the multimerization of the CD95 (Fas/APO-1) (under UVB/C radiation) which is responsible for the cell apoptosis process. Considering the mentioned reasons, the UV radiation could significantly trigger the cell apoptosis. This is noteworthy since the cell apoptosis is followed by significant morphological changes [44]. It is believed that the onset of the apoptosis is

accompanied by the reorganization of the microtubules as well as intermediate and actin filaments [44, 45]. This provides significant evidence for our reasoning that cell apoptosis is the main reason for rejecting the initial hypothesis of our research.

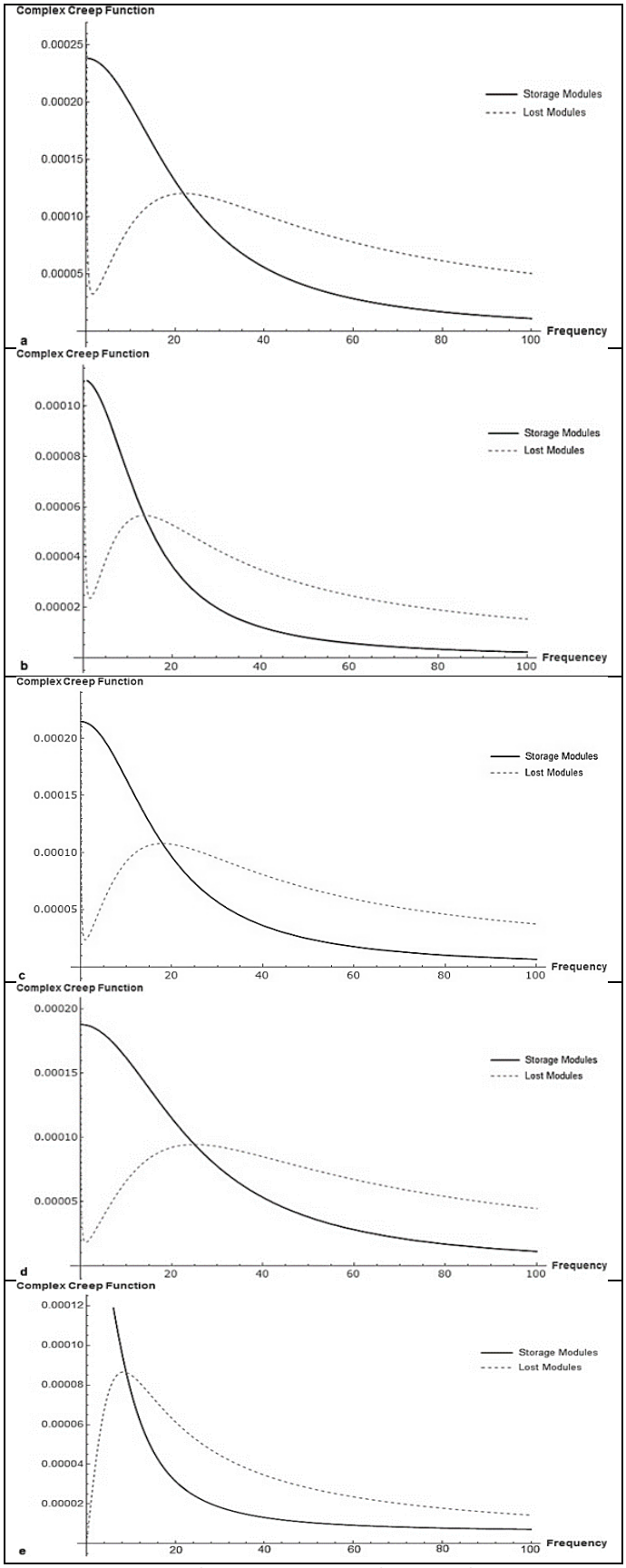

Figure 6. Diagrams of the creep complex function of the samples; a) Diagram of the Control group; b) Diagram of the UVC38 group; c) Diagram of the UVC60 group; d) Diagram of the UVC120 group; e) Diagram of the UVB38 group.

Table 2. Numerical values of the stiffness, loss, and storage modulus of experimental groups

	Control	UVB38	UVC38	UVC60	UVC120
D' $m \cdot \mu N^{-1}$	1.6×10^{-5}	6.62×10^{-6}	2.85×10^{-6}	9.82×10^{-6}	1.6×10^{-5}
D" $m \cdot \mu N^{-1}$	6.2×10^{-5}	8.86×10^{-6}	1.92×10^{-5}	4.7×10^{-5}	5.2×10^{-5}
|D*| $m \cdot \mu N^{-1}$	4.1×10^{-9}	10^{-10}	2.3×10^{-9}	2.4×10^{-9}	3×10^{-9}

5. Conclusion

According to the previous studies, the deformation and many of the other mechanical properties of the cell are related to the cytoskeleton of the cell [46-50]. In previous studies, it was also suggested that the mechanical properties of the cell such as deformation that are attributed to cytoskeleton are indeed related to three types of polymer proteins called actin filaments, tubulin filaments, and intermediate filaments [51-54]. Nowadays, we know that UV radiation has many adverse effects such as accelerating skin aging and wrinkling. Indeed, UV radiation causes the formation of reactive oxygen species (ROS), which eventually leads to the above-mentioned effects in the cell [55-57]. Such free radicals cause changes in the structure of cytoskeleton of the cells as well as their structural proteins through causing oxidative damage which can culminate in the reorganization of the cell structure [8, 58-61]. Therefore, it can be concluded that reorganization of the filaments and structural proteins of the cytoskeleton justifies the reduced deformation.

Furthermore, concerning the stiffness of the cells, it is observed that their stiffness has significantly decreased upon radiation in comparison to the control group. This result is in accordance with the results obtained from the research conducted by Bertrand Vileno et *al*. [13] for the effect of UVC on the stiffness of skin fibroblast cells. They found a significant reduction in Young modulus of cells under the exposure of UVC ($0.1 mW/cm^2$, 120s) which changed the Young modulus of cells from 1 to 25% representing nearly 75% reduction in the value of cell's Young modulus. However, there are other experiments which have found opposite results. For instance, in a research conducted by John P. Hale et *al*. [62] on the effect of two types of free oxygen radicals on the elasticity of red blood cells, they found that such free radicals caused enhanced elastic modulus of the cell membrane. Also, in another study conducted by Devasier Benneta and Sanghyo Kim [16], the experiment showed a significant increase (40-60 kPa during the 5 minutes of UVC radiation) in the cell's Young modulus after radiation. Additionally, Krysta Biniek et *al*. [22] revealed the constant stiffness of skin cells under UVB radiation. The reason for such contrary results may arise from several factors including the elastic model assumption which has been used in the mentioned research. Further, other critical factors such as different cell samples and radiation durations can cause such a difference in the reported findings.

Also, the reduction of stiffness for the sample from the group UVB38 was far higher which was contrary to our hypothesis suggesting the effect of higher frequencies on reducing stiffness of the cell. Further, stiffness diminished to a lesser extent in the radiated groups of UVC38, UVC60, and UVC120 as the radiation duration increased. This result is important since according to our

primary hypothesis, we expected greater destruction of the cell structure upon increasing the radiation duration. As such, we expected a reduction of stiffness to a higher extent, while it was not obtained in our results. This is possibly due to the cell apoptosis which can suppress the loss of the cell deformation. According to previous studies, UV radiation can initiate the process of cell death due to the changes in the structure of actin filaments [63, 64].

Future research could assess the cytoskeletal structure of the cells after short-term radiation to test our reasoning.

6. References

[1] Paul, W., and P. Sharma, C., 2015, Advances in Wound Healing Materials: Science and Skin Engineering.

[2] Lai-Cheong, J. E., and McGrath, J. A., 2017, "Structure and function of skin, hair and nails," Medicine, 45(6), pp. 347-351.

[3] Gallo, R. L., 2017, "Human Skin Is the Largest Epithelial Surface for Interaction with Microbes," J Invest Dermatol, 137(6), pp. 1213-1214.

[4] Farage, M. A., Miller, K. W., and Maibach, H. I., 2009, Textbook of aging skin, Springer Science & Business Media.

[5] Panich, U., Sittithumcharee, G., Rathviboon, N., and Jirawatnotai, S., 2016, "Ultraviolet Radiation-Induced Skin Aging: The Role of DNA Damage and Oxidative Stress in Epidermal Stem Cell Damage Mediated Skin Aging," Stem Cells Int, 2016, p. 7370642.

[6] D'Orazio, J., Jarrett, S., Amaro-Ortiz, A., and Scott, T., 2013, "UV radiation and the skin," Int J Mol Sci, 14(6), pp. 12222-12248.

[7] Watson, M., Holman, D. M., and Maguire-Eisen, M., 2016, "Ultraviolet Radiation Exposure and Its Impact on Skin Cancer Risk," Semin Oncol Nurs, 32(3), pp. 241-254.

[8] Svobodová, A., Psotová, J., and Walterová, D., 2003, "Natural phenolics in the prevention of UV-induced skin damage. A review," Biomedical Papers, 147(2), pp. 137-145.

[9] Martens, M. C., Seebode, C., Lehmann, J., and Emmert, S., 2018, "Photocarcinogenesis and Skin Cancer Prevention Strategies: An Update," Anticancer Res, 38(2), pp. 1153-1158.

[10] Krutmann, J., Bouloc, A., Sore, G., Bernard, B. A., and Passeron, T., 2017, "The skin aging exposome," J Dermatol Sci, 85(3), pp. 152-161.

[11] Gandhi, S. A., and Kampp, J., 2015, "Skin Cancer Epidemiology, Detection, and Management," Med Clin North Am, 99(6), pp. 1323-1335.

[12] Dakup, P., and Gaddameedhi, S., 2017, "Impact of the Circadian Clock on UV-Induced DNA Damage Response and Photocarcinogenesis," Photochem Photobiol, 93(1), pp. 296-303.

[13] Vileno, B., Lekka, M., Sienkiewicz, A., Jeney, S., Stoessel, G., Lekki, J., Forro, L., and Stachura, Z., 2007, "Stiffness alterations of single cells induced by UV in the presence of nanoTiO2," Environ Sci Technol, 41(14), pp. 5149-5153.

[14] Dupont, E., Gomez, J., and Bilodeau, D., 2013, "Beyond UV radiation: a skin under challenge," Int J Cosmet Sci, 35(3), pp. 224-232.

[15] Cadet, J., and Douki, T., 2018, "Formation of UV-induced DNA damage contributing to skin cancer development," Photochem Photobiol Sci, 17(12), pp. 1816-1841.

[16] Bennet, D., and Kim, S., 2015, "Evaluation of UV radiation-induced toxicity and biophysical changes in various skin cells with photo-shielding molecules," Analyst, 140(18), pp. 6343-6353.

[17] Querleux, B., 2016, Computational Biophysics of the Skin, Jenny Stanford Publishing.

[18] Weihermann, A. C., Lorencini, M., Brohem, C. A., and de Carvalho, C. M., 2017, "Elastin structure and its involvement in skin photoageing," Int J Cosmet Sci, 39(3), pp. 241-247.

[19] Watson, R. E., Gibbs, N. K., Griffiths, C. E., and Sherratt, M. J., 2014, "Damage to skin extracellular matrix induced by UV exposure," Antioxid Redox Signal, 21(7), pp. 1063-1077.

[20] Nishimori, Y., Edwards, C., Pearse, A., Matsumoto, K., Kawai, M., and Marks, R., 2001, "Degenerative alterations of dermal collagen fiber bundles in photodamaged human skin and UV-irradiated hairless mouse skin: possible effect on decreasing skin mechanical properties and appearance of wrinkles," J Invest Dermatol, 117(6), pp. 1458-1463.

[21] Takema, Y., and Imokawa, G., 1998, "The effects of UVA and UVB irradiation on the viscoelastic properties of hairless mouse skin in vivo," Dermatology, 196(4), pp. 397-400.

[22] Biniek, K., Levi, K., and Dauskardt, R. H., 2012, "Solar UV radiation reduces the barrier function of human skin," Proc Natl Acad Sci U S A, 109(42), pp. 17111-17116.

[23] Lekka, M., Pogoda, K., Gostek, J., Klymenko, O., Prauzner-Bechcicki, S., Wiltowska-Zuber, J., Jaczewska, J., Lekki, J., and Stachura, Z., 2012, "Cancer cell recognition--mechanical phenotype," Micron, 43(12), pp. 1259-1266.

[24] Efremov, Y. M., Wang, W. H., Hardy, S. D., Geahlen, R. L., and Raman, A., 2017, "Measuring nanoscale viscoelastic parameters of cells directly from AFM force-displacement curves," Sci Rep, 7(1), p. 1541.

[25] Weaver, D. S., 2000, "Skeletal tissue mechanics," American Journal of Physical Anthropology, 112(3), pp. 435-436.

[26] Zheng, Y., Nguyen, J., Wei, Y., and Sun, Y., 2013, "Recent advances in microfluidic techniques for single-cell biophysical characterization," Lab Chip, 13(13), pp. 2464-2483.

[27] Lee, G. Y., and Lim, C. T., 2007, "Biomechanics approaches to studying human diseases," Trends Biotechnol, 25(3), pp. 111-118.

[28] Suresh, S., Spatz, J., Mills, J. P., Micoulet, A., Dao, M., Lim, C. T., Beil, M., and Seufferlein, T., 2015, "Reprint of: Connections between single-cell biomechanics and human disease states: gastrointestinal cancer and malaria," Acta Biomater, 23 Suppl, pp. S3-15.

[29] Hayot, C. M., Forouzesh, E., Goel, A., Avramova, Z., and Turner, J. A., 2012, "Viscoelastic properties of cell walls of single living plant cells determined by dynamic nanoindentation," J Exp Bot, 63(7), pp. 2525-2540.

[30] Hecht, F. M., Rheinlaender, J., Schierbaum, N., Goldmann, W. H., Fabry, B., and Schaffer, T. E., 2015, "Imaging viscoelastic properties of live cells by AFM: power-law rheology on the nanoscale," Soft Matter, 11(23), pp. 4584-4591.

[31] Kollmannsberger, P., and Fabry, B., 2007, "High-force magnetic tweezers with force feedback for biological applications," Rev Sci Instrum, 78(11), p. 114301.

[32] Wang, Y.-l., and Discher, D. E., 2007, Cell mechanics, Academic press.

[33] Parvanehpour, N., Shojaei, S., Khorramymehr, S., Goodarzi, V., Hejazi, F., and Rezaei, V. F., 2018, "Diabetes can change the viscoelastic properties of lymphocytes," Prog Biomater, 7(3), pp. 219-224.

[34] Heydarian, A., Khorramymehr, S., and Vasaghi-Gharamaleki, B., 2019, "Short-term effects of X-ray on viscoelastic properties of epithelial cells," Proc Inst Mech Eng H, 233(5), pp. 535-543.

[35] Rekik, A., Nguyen, T. T. N., and Gasser, A., 2016, "Multi-level modeling of viscoelastic microcracked masonry," International Journal of Solids and Structures, 81, pp. 63-83.

[36] Lim, C. T., Zhou, E. H., and Quek, S. T., 2006, "Mechanical models for living cells--a review," J Biomech, 39(2), pp. 195-216.

[37] Saunders, D. W., 1978, "Creep and relaxation of nonlinear viscoelastic materials," Polymer, 19(1), p. 118.

[38] Lundström, R., 1984, "Local vibrations—Mechanical impedance of the human hand's glabrous skin," Journal of Biomechanics, 17(2), pp. 137-144.

[39] Lee, C. H., Wu, S. B., Hong, C. H., Yu, H. S., and Wei, Y. H., 2013, "Molecular Mechanisms of UV-Induced Apoptosis and Its Effects on Skin Residential Cells: The Implication in UV-Based Phototherapy," Int J Mol Sci, 14(3), pp. 6414-6435.

[40] Gentile, M., Latonen, L., and Laiho, M., 2003, "Cell cycle arrest and apoptosis provoked by UV radiation-induced DNA damage are transcriptionally highly divergent responses," Nucleic Acids Res, 31(16), pp. 4779-4790.

[41] Salucci, S., Burattini, S., Battistelli, M., Baldassarri, V., Maltarello, M. C., and Falcieri, E., 2012, "Ultraviolet B (UVB) irradiation-induced apoptosis in various cell lineages in vitro," Int J Mol Sci, 14(1), pp. 532-546.
[42] Pustišek, N., and Šitum, M., 2011, "UV-radiation, apoptosis and skin," Collegium antropologicum, 35(2), pp. 339-341.
[43] Kulms, D., Dussmann, H., Poppelmann, B., Stander, S., Schwarz, A., and Schwarz, T., 2002, "Apoptosis induced by disruption of the actin cytoskeleton is mediated via activation of CD95 (Fas/APO-1)," Cell Death Differ, 9(6), pp. 598-608.
[44] Povea-Cabello, S., Oropesa-Avila, M., de la Cruz-Ojeda, P., Villanueva-Paz, M., de la Mata, M., Suarez-Rivero, J. M., Alvarez-Cordoba, M., Villalon-Garcia, I., Cotan, D., Ybot-Gonzalez, P., and Sanchez-Alcazar, J. A., 2017, "Dynamic Reorganization of the Cytoskeleton during Apoptosis: The Two Coffins Hypothesis," Int J Mol Sci, 18(11).
[45] Mills, J. C., Stone, N. L., and Pittman, R. N., 1999, "Extranuclear apoptosis. The role of the cytoplasm in the execution phase," J Cell Biol, 146(4), pp. 703-708.
[46] Phillip, J. M., Aifuwa, I., Walston, J., and Wirtz, D., 2015, "The Mechanobiology of Aging," Annu Rev Biomed Eng, 17, pp. 113-141.
[47] Fletcher, D. A., and Mullins, R. D., 2010, "Cell mechanics and the cytoskeleton," Nature, 463(7280), pp. 485-492.
[48] Schillers, H., Walte, M., Urbanova, K., and Oberleithner, H., 2010, "Real-time monitoring of cell elasticity reveals oscillating myosin activity," Biophys J, 99(11), pp. 3639-3646.
[49] Bai, G., Li, Y., Chu, H. K., Wang, K., Tan, Q., Xiong, J., and Sun, D., 2017, "Characterization of biomechanical properties of cells through dielectrophoresis-based cell stretching and actin cytoskeleton modeling," Biomed Eng Online, 16(1), p. 41.
[50] Wang, X., Liu, H., Zhu, M., Cao, C., Xu, Z., Tsatskis, Y., Lau, K., Kuok, C., Filleter, T., McNeill, H., Simmons, C. A., Hopyan, S., and Sun, Y., 2018, "Mechanical stability of the cell nucleus - roles played by the cytoskeleton in nuclear deformation and strain recovery," J Cell Sci, 131(13).
[51] Kletter, Y., Riklis, I., Shalit, I., and Fabian, I., 1991, "Enhanced repopulation of murine hematopoietic organs in sublethally irradiated mice after treatment with ciprofloxacin," Blood, 78(7), pp. 1685-1691.
[52] Janmey, P. A., 1991, "Mechanical properties of cytoskeletal polymers," Current Opinion in Cell Biology, 3(1), pp. 4-11.
[53] Lele, T. P., Dickinson, R. B., and Gundersen, G. G., 2018, "Mechanical principles of nuclear shaping and positioning," J Cell Biol, 217(10), pp. 3330-3342.
[54] Dogterom, M., and Koenderink, G. H., 2019, "Actin-microtubule crosstalk in cell biology," Nat Rev Mol Cell Biol, 20(1), pp. 38-54.
[55] Emri, G., Paragh, G., Tosaki, A., Janka, E., Kollar, S., Hegedus, C., Gellen, E., Horkay, I., Koncz, G., and Remenyik, E., 2018, "Ultraviolet radiation-mediated development of cutaneous melanoma: An update," J Photochem Photobiol B, 185, pp. 169-175.
[56] McDaniel, D., Farris, P., and Valacchi, G., 2018, "Atmospheric skin aging-Contributors and inhibitors," J Cosmet Dermatol, 17(2), pp. 124-137.
[57] Azzouz, D., Khan, M. A., Sweezey, N., and Palaniyar, N., 2018, "Two-in-one: UV radiation simultaneously induces apoptosis and NETosis," Cell Death Discov, 4, p. 51.
[58] Schmid, I., 2012, Flow Cytometry: Recent Perspectives, BoD–Books on Demand.
[59] Shi, K., Gao, Z., Shi, T. Q., Song, P., Ren, L. J., Huang, H., and Ji, X. J., 2017, "Reactive Oxygen Species-Mediated Cellular Stress Response and Lipid Accumulation in Oleaginous Microorganisms: The State of the Art and Future Perspectives," Front Microbiol, 8, p. 793.
[60] De Jager, T. L., Cockrell, A. E., and Du Plessis, S. S., 2017, "Ultraviolet Light Induced Generation of Reactive Oxygen Species," Adv Exp Med Biol, 996, pp. 15-23.
[61] Almeida-Marrero, V., van de Winckel, E., Anaya-Plaza, E., Torres, T., and de la Escosura, A., 2018, "Porphyrinoid biohybrid materials as an emerging toolbox for biomedical light management," Chemical Society Reviews, 47(19), pp. 7369-7400.
[62] Hale, J. P., Winlove, C. P., and Petrov, P. G., 2011, "Effect of hydroperoxides on red blood cell membrane mechanical properties," Biophys J, 101(8), pp. 1921-1929.
[63] Suarez-Huerta, N., Mosselmans, R., Dumont, J. E., and Robaye, B., 2000, "Actin depolymerization and polymerization are required during apoptosis in endothelial cells," Journal of Cellular Physiology, 184(2), pp. 239-245.
[64] Grzanka, D., Domaniewski, J., Grzanka, A., and Zuryn, A., 2006, "Ultraviolet radiation (UV) induces reorganization of actin cytoskeleton in CHOAA8 cells," Neoplasma, 53(4), pp. 328-332.